10th AIAA/CEAS Aeroacoustics Conference
10-12 May, 2004 / Manchester, United Kingdom

AIAA-2004-2979

NUMERICAL PREDICTION OF CHEVRON NOZZLE NOISE REDUCTION USING WIND-MGBK METHODOLOGY

W. A. Engblom*, A. Khavaran†, J. Bridges‡
NASA Glenn Research Center, 21000 Brookpark Rd., Cleveland, OH 44135

ABSTRACT

Numerical predictions for single-stream chevron nozzle flow performance and farfield noise production are presented. Reynolds Averaged Navier Stokes (RANS) solutions, produced via the WIND flow solver, are provided as input to the MGBK code for prediction of farfield noise distributions. This methodology is applied to a set of sensitivity cases involving varying degrees of chevron inward bend angle relative to the core flow, for both cold and hot exhaust conditions.

The sensitivity study results illustrate the effect of increased chevron bend angle and exhaust temperature on enhancement of fine-scale mixing, initiation of core breakdown, nozzle performance, and noise reduction. Direct comparisons with experimental data, including stagnation pressure and temperature rake data, PIV turbulent kinetic energy fields, and 90° observer farfield microphone data are provided. Although some deficiencies in the numerical predictions are evident, the correct farfield noise spectra trends are captured by the WIND-MGBK method, including the noise reduction benefit of chevrons. Implications of these results to future chevron design efforts are addressed.

INTRODUCTION

One of the primary goals of NASA's Quiet Aircraft Technology (QAT) program is to reduce the Effective Perceived Noise Level (EPNL) for commercial aircraft noise by 10 dB by 2007. Jet engine noise, of course, represents the bulk of this noise impact. Several noise-reducing nozzle concepts have been designed in recent years. For such concepts to be considered for installation in commercial aircraft, thrust penalties associated with these nozzles must be minimized.

There is significant potential for chevron nozzles to provide such noise reductions. Researchers have experimentally demonstrated that certain chevron nozzle configurations can provide nearly 3 dB of noise reduction during takeoff with less than 0.5% thrust loss during cruise [1,2]. General Electric has demonstrated ~2.5 EPNdB reductions at takeoff for a full-scale CF34-8C (see Fig. 1).

There have been several research efforts [3-6] focused on applying Reynolds-Averaged Navier-Stokes (RANS) flow solvers to chevron nozzle flows to assess the potential of such codes to simulate the resulting mixing, core breakdown, and noise production. These efforts have demonstrated that RANS methods can provide credible estimates of the chevron effect but are not precise due to limitations of the turbulence models.

The relative success of previous research efforts to quantify the chevron effect is the impetus for the current research effort. The main objective here is to develop a relatively robust numerical methodology for a quick and meaningful assessment of chevron performance, both noise reduction potential as well as thrust performance. The numerical methodology must demonstrate the correct sensitivities (e.g., the effect of various geometric modifications on noise reduction). The ultimate goal is to use this methodology as a guide to help chevron designers prior to hardware fabrication.

METHODOLOGY

Configurations

The main objective here is to apply the numerical method to a set of nozzles for which sufficient experimental data exists (i.e., stagnation pressure/temperature rakes, PIV data, and microphone data), and to assess the validity of the numerical approach (i.e., aerodynamic mixing and noise production). A subset of chevron nozzles tested using the Small Hot Jet Acoustic Rig (SHJAR) at NASA Glenn Research Center by Bridges and Brown [7] was chosen, and are shown in Fig. 2. These SHJAR nozzles are single-stream, 6-chevron geometries, and were tested using both cold and hot exhaust streams.

The four SHJAR nozzles evaluated are identical except for the inward bend angle of the chevron petals. Fig. 3 illustrates the SMC001 SHJAR nozzle and the key dimension (internal tip-to-tip distance) used to control the amount of chevron inward bending using a Computer Aided Design (CAD) package. The CAD models were generated using engineering drawings and measurements taken from the actual test articles. Table 1 summarizes the nozzle geometries evaluated. The

*Engineering Specialist, The Aerospace Corporation, Senior Member AIAA
†Senior Research Engineer, QSS, Senior Member AIAA
‡Senior Research Scientist, NASA Glenn Research Center, Senior Member AIAA

"SPECIAL" case was not evaluated experimentally, and so does not have a numerical nozzle designation.

Table 1. Chevron nozzle geometries

Nozzle Designation	Bend Angle (deg)	Tip-to-tip Distance (in)
SMC000	N/A	N/A
SMC005	0	2.17
SMC001	5	2.00
SPECIAL	11	1.86
SMC006	17.7	1.69

Note: SMC000 is the baseline round nozzle

Grid Resolution

Three-dimensional grids were constructed with grid sequencing and parallel computation in mind. Two symmetry planes are used to limit the domain to one-half of a single chevron (i.e., a 30° pie sector). Fig. 4 shows a sample grid slice for SMC001. The block boundaries are also evident. The overall domain (not shown here) extends 20 core diameters radially, and 30 core diameters axially. A Gridgen template based on the baseline case (SMC001) was used to minimize the effort required to grid the remaining cases. Each grid consists of ~2.0 million cells and 23 zones. The grids are sequenced from coarse to medium to fine, with factor of 8 increases in cell number between each level (i.e., x2 along I-, J-, and K- directions).

The internal nozzle viscous wall surfaces are resolved with 5.0E-05 inch initial spacing, which resulted in a maximum $y+$ of approximately 1. A grid sensitivity study, not discussed in detail herein, was conducted for each chevron nozzle configuration. The differences between medium and fine grid converged solutions were negligible based on comparisons for farfield noise production and centerline velocity distribution. As a result, a sufficient level of grid independence was obtained.

Run Matrix

Table 2 provides typical cold exhaust conditions recorded during the experiments [7], including: supply plenum stagnation pressure (P_o) and stagnation temperature (T_o), and ambient static pressure (P_∞) and static temperature (T_∞). The design Mach number at the nozzle exit is also provided. The freestream is quiescent in all cases. Each of the four chevron geometries is evaluated for both exhaust conditions.

Table 2. Typical Flow conditions

Type	P_O (psia)	T_O (R)	P_∞ (psia)	T_∞ (R)	Design Mach
Cold	25.84	515.6	14.18	504.3	0.967
Hot	17.68	1409.7	14.40	505.6	0.591

Numerical Scheme

The numerical method for evaluating a given chevron nozzle case consists of two steps: 1) obtain RANS solution using WIND code, 2) obtain farfield noise spectrum using MGBK code.

WIND Description

The RANS solution is generated using WIND (Version 5) [8] -- a flow solver provided by the NPARC Alliance, a partnership of NASA Glenn Research Center, USAF Arnold Engineering Development Center (AEDC), and the Boeing Company. WIND is a multi-block structured-grid finite volume solver that offers multi-purpose capabilities. For the current effort, true second-order (i.e., cell stretching included) Roe flux-difference splitting was implemented. The two-equation shear-stress transport (SST) turbulence model from Menter [9] was chosen based on the success of previous researchers [10-11] when applying SST to characterizing the turbulence fields generated by dual stream nozzles and mixing devices. SST is a blended combination of κ-ω (near walls) and κ-ε (away from walls). Stagnation conditions are maintained for both the nozzle supply plenum and the freestream boundaries. That is, no co-flow was necessary for numerical convergence. Freestream static pressure is fixed at the outflow boundary.

WIND's default implicit scheme (i.e., spatial approximate factorization), was used to drive the solutions to steady-state (5 iterations per zone per cycle; CFL = 0.5) for the cold exhaust cases. Sufficient convergence was defined as obtaining < 0.1% variation in nozzle mass flow and centerline velocity distribution over approx. 500 cycles (based on limit cycle observed in residual histories). However, the default scheme did not produce satisfactory convergence (i.e., typically > 2% variation in nozzle mass flow) for hot exhaust cases despite numerous attempts at adjusting scheme parameters. For the hot exhaust cases, the Gauss-Seidel subiteration scheme (30 subiterations, 0.0001 step convergence tolerance) was found to provide sufficient convergence. It is thought that spatial factorization error, coupled with high temperature

gradients in the initial mixing region, is perhaps the source of the convergence problem.

MGBK Description

The MGBK code as used in the current farfield noise prediction has its origins in a unified aeroacoustics model (MGB), originally developed by the General Electric company [12]. The governing equation describing the propagation as well as the source of sound is Lilley's equation. This equation is linearized about a unidirectional transversely sheared base flow. The non-linear terms, second-order in turbulent fluctuations, are moved to the right-hand side of the equation and identified as the source. The sources considered in the following predictions are the so-called self- and shear-noise terms. Both sources are second-order in velocity fluctuations and are modeled using appropriate description of the statistical properties of turbulence.

The Green's function governing the propagation of sound is a high-frequency asymptotic solution [13]. A detailed comparison of this solution with the ray-acoustic as well as exact Green's function [14] shows that it remains accurate in the mid angle range (i.e., 60°-120°) and down to a Strouhal number of 0.5.

A RANS solution, including mean flowfield and turbulence, is used to calculate the noise source strength, its spectral characteristics, and the propagation Green's function. Source strength is shown to scale as the 7/2 power of turbulence kinetic energy (TKE). Time- and length-scales of two-point correlation functions are calculated from TKE and its dissipation rate [15].

RESULTS

Cold Exhaust Cases

A direct comparison between WIND and SHJAR stagnation pressure rake data for the SMC001 (5° bend angle) case is provided in Fig. 5. Stagnation pressure contours are shown for eight crossflow slices at downstream X/D_e values of 0.1, 0.2, 0.5, 1, 2, 5, 10, and 20. X is the axial distance starting from the chevron trailing edge and D_e is the nominal core diameter of 2 inches for all cases illustrated here. Note that D_e is the same as the internal chevron tip-to-tip distance for SMC001.

The results compare quite well qualitatively (i.e., for contour patterns) and reasonably well quantitatively. The numerical results somewhat underpredict mixing based on the thickness of the shear layers evident for the near-field slices. Note that the experimental rake resolves the slices using a 10 x 10 Cartesian grid, and will tend to exaggerate the shear layer thickness at the earliest cuts. The most glaring difference is in the vicinity of the centerline for $X/D_e = 5$ and 10, indicating that the numerics significantly overpredict the potential core length. This is not a surprise based on an observation from Birch et al that the standard κ-ε model overpredicts core length by about 15% for axisymmetric jets [3]. There is more discussion on the core length disagreement below. Note that the WIND results overpredict mixing for the furthest downstream cut (i.e., the predicted mixing "catches up" with the experimental results in the asymptotic region) between 10 and 20 diameters downstream.

Fig. 6 illustrates comparisons between WIND and SHJAR PIV data for the turbulent kinetic energy (TKE) field along longitudinal slices, for four SMC cold exhaust cases. These comparisons are limited to $X/D_e > 1$ due to concerns over the quality of the experimental data within one diameter of the nozzle exit. The slices are along the plane of symmetry thru the middle of each chevron petal. The topmost comparison is for the round jet (no chevron) case, SMC000. The chevron inward bend angle increases from the second to fourth picture. The TKE distributions agree reasonably well with respect to the range and extent of the TKE distributions. However, as chevron angle is increased, there is a more pronounced under prediction of the peak TKE levels within the upstream portion of the shear layer, and a related over prediction of the potential core length. Nevertheless, the numerics demonstrate the correct trend of decreasing core length with increasing chevron bend angle.

Note that the experimental SMC005 plot indicates two subtle local peaks in TKE along the shear layer. The first thought is that this subtle effect may be due to infant shocks (i.e., shock cell structure) created by an imperfect expansion at the nozzle trailing edge, since the experimental uncertainties in this region are estimated to be within a few percent. More discussion on this topic will follow for the hot exhaust cases.

The differences between the WIND predictions and SHJAR rake data for the cold exhaust centerline velocity profiles (and related core length over prediction) are illustrated in Fig. 7. The three experimental results for chevron nozzle cases are included. The same cases, plus one purely numerical case (SPECIAL), are also plotted. The round jet cases

have been excluded for clarity. There is a systematic reduction in core length with increasing chevron inward bend angle in both data sets (core breakdown initiation moves forward ~3 core diameters). Moreover, there is approximately the same shift in core length in both data sets.

Details of the predicted TKE near the nozzle exit are shown in Fig. 8 for the four chevron geometries (i.e., different bend angles). As in Fig. 6, the slices are again along the plane of symmetry thru the middle of each chevron, but include the first diameter just downstream of the trailing edge. The maximum value of TKE within the field increases and moves upstream with increasing bend angle. The vertical width of the mixing region also increases noticeably with bend angle. This figure indicates that increasing the inward bend angle intensifies fine scale turbulence effects near the nozzle exit. However, it can be argued that the SPECIAL case results are not entirely consistent with these trends.

Table 3 summarizes key nozzle performance metrics for the cold exhaust cases, including the mass flow, thrust, gross thrust coefficient, and mass-flux averaged divergence efficiency. The later two parameters are defined in Eqns 1 and 2. Note that the conventional definition of divergence efficiency requires the nozzle wall divergence angle, and is most appropriate for round jets. The divergence efficiency in Table 3 has been formulated to measure how much of the thrust loss in efficiency is related to the loss of axial flow (i.e., flow divergence) at the nozzle exit. This parameter is defined analogously to the conventional divergence efficiency, except that the divergence is computed locally along the nozzle exit and mass-flux averaged.

$$Cf_g = \frac{Th_{actual}}{\dot{m}_{actual}\, V_{ideal}} \qquad (1)$$

$$\eta_{divergence} = \left(\sum_i \dot{m}_i \left(\frac{V_{axial}}{V_{total}} \right)_i \right) \Big/ \sum_i \dot{m}_i \qquad (2)$$

Note that the SMC001 chevron nozzle is precisely the SMC000 round jet with chevrons "cut-out". This results in a larger effective exit area and a related increase in massflow and thrust since these are converging nozzles. Note that as chevron inward bend angle increases from 0° to 17.7°, the effective exit area, and mass flow and thrust, are gradually reduced. The gross thrust coefficient (Eq. 1) is almost constant, dropping only ~1% with increasing chevron bend angle. A portion of the thrust loss for the larger bend angle cases is apparently related to divergence efficiency, based on the correlation of divergence efficiencies and gross thrust coefficient. Other primary sources of thrust loss are viscous losses, and the degree of overexpansion or underexpansion at the nozzle exit. The larger bend angle cases exhibit a slight *vena contracta* effect, created by the nozzle inward divergence angle. The latter results in core flow acceleration and expansion downstream of the nozzle exit (i.e., the nozzle flow is underexpanded).

Table 3. Nozzle Performance (Cold exhaust)

SMC#	000	005	001	SPC	006
Bend Angle (deg)	N/A	0	5	11	17.7
Mass Flow (lbm/s)	1.881	2.328	2.160	2.022	1.870
Thrust (lbf)	57.07	70.37	65.34	60.95	56.07
Cf,g*	0.984	0.980	0.982	0.978	0.972
Divergence Efficiency**	0.999	0.999	0.994	0.977	0.949

* Eq. 1, gross thrust coeffcient (based on Videal = 993 ft/s)
**Eq. 2, mass-flux weighted divergence efficiency

MGBK-generated farfield noise predictions for an observer at 90°, based on these WIND RANS solutions, are directly compared with SHJAR acoustic measurements in Fig. 9. Some qualitative and quantitative trends are captured by the WIND-MGBK methodology. In both data sets the sound spectral density is being redistributed from low frequency to high frequency as chevron inward bend angle increases. The spectra crossover point (i.e., the frequency at which the noise level is essentially stable for the set of chevron configurations) agrees reasonably well between the experiments (~4 kHz) and the numerics (~7 kHz). As the bend angle increases from 0° to 17.7°, there is a fairly consistent delta-dB of ~5 dB in the experiments. The numerics predict similar delta-dB trends with ~5 dB or less at low frequencies, and ~5 dB at high frequencies. The general trends are not surprising. The fine scale turbulence levels near the exit intensifies as chevron bend angle increases, which in turn leaves less energy available for the relatively low frequency, core breakdown process.

Hot Exhaust Cases

A turbulent Prandtl number of 0.7 (rather than the cold exhaust case value of 0.9) was chosen for all

simulations herein. This choice has been shown to improve numerical simulation of round jets [16].

A direct comparison between WIND and SHJAR stagnation temperature rake data for the SMC001 (5° bend angle) case is provided in Fig. 10. Stagnation temperature contours are plotted, as was shown for the cold exhaust cases, for eight crossflow slices at downstream X/D_e values of 0.1, 0.2, 0.5, 1, 2, 5, 10, and 20.

As with the cold exhaust cases, the results compare quite well qualitatively (i.e., for contour patterns) and reasonably well quantitatively. Again, the numerical results somewhat underpredict mixing in the initial shear layer region, and consequently overpredict core length. Also, the predicted mixing "catches up" with the experimental results in the asymptotic region, between 10 and 20 diameters downstream.

Fig. 11 illustrates comparisons between WIND and SHJAR PIV data for the turbulent kinetic energy (TKE) field along longitudinal slices, for four SMC hot exhaust cases. Again, these comparisons are limited to $X/D_e > 1$ due to concerns over the quality of the experimental data within one diameter of the nozzle exit. The slices are along the plane of symmetry thru the middle of each chevron petal. The TKE distributions agree reasonably well with respect to the range and extent of the TKE distributions. However, as chevron angle is increased, there is significant under prediction of the peak TKE levels within the upstream portion of the shear layer, and a related over prediction of the core length. Nevertheless, the numerics demonstrate the correct trend of decreasing core length with increasing chevron bend angle.

It should be noted that both the experimental and numerical SMC000 and SMC005 plots indicate two very subtle, local peaks in TKE along the shear layer. They cannot be attributed to infant shocks, as with the cold exhaust. We see no plausible, physical explanation for a second local TKE maximum in either the experiments or numerics, and assume they are related to the interpolation error of the experimental data, and a lack of rigorous numerical convergence, respectively.

The differences between the WIND predictions and SHJAR rake data for the hot exhaust centerline velocity profiles (and related core length over prediction) are illustrated in Fig. 12. There is again systematic reduction in core length with increasing chevron inward bend angle in both data sets (core breakdown initiation moves forward ~2.5 core diameters). Moreover, there is approximately the same shift in core length between experiment and numerics.

Enhanced details of the TKE near the nozzle exit and for the four chevron geometries (i.e., different bend angles) are provided in Fig. 13. The trends are similar to the cold exhaust results shown earlier. The maximum value of TKE within the field consistently increases and tends to move upstream, with increasing bend angle. The vertical width of the mixing region also increases noticeably with bend angle. Increasing inward bend angle intensifies fine scale turbulence effects in the near-field.

Table 4 summarizes key nozzle performance metrics for the hot exhaust cases. The trends are quite similar to those seen for the cold exhaust results, and earlier discussion following Table 3 could be repeated here. However, there the gross thrust coefficient is nearly unchanged despite the variation in divergence efficiency. Due to a relatively small pressure head (see Table 1) for the hot exhaust cases, there is significant sensitivity (i.e., tenths of percent) in the thrust and divergence coefficients to small changes in the assumed ambient pressure. Although there is some ambiguity in the gross thrust coefficient comparisons, the results again suggest that the addition of the chevrons do not represent a major performance penalty.

Table 4. Nozzle Performance (Hot exhaust)

SMC#	000	005	001	SPC	006
Bend Angle (deg)	N/A	0	5	11	17.7
Mass Flow (lbm/s)	0.615	0.760	0.695	0.641	0.581
Thrust (lbf)	18.72	23.12	21.16	19.58	17.71
Cf,g*	0.982	0.980	0.981	0.985	0.983
Divergence Efficiency**	0.999	1.000	0.997	0.985	0.962

* Eq. 1, gross thrust coefficient (based on Videal = 998.6 ft/s)
**Eq. 2, mass-flux weighted divergence efficiency

MGBK-generated farfield noise predictions for an observer at 90°, based on the WIND RANS solutions, are directly compared with SHJAR acoustic measurements in Fig. 14. Some qualitative and quantitative trends are again captured by the WIND-MGBK methodology. In both data sets the spectral density is more-or-less being redistributed from low frequency to high frequency as chevron inward bend angle increases. The spectra crossing-point of ~6 kHz from the experiments is reasonably predicted at ~10

kHz. As the bend angle increases from 0° to 17.7°, there is a fairly consistent delta-dB of ~5 dB in the experiments. The numerics also predict ~5 dB or more increase at high frequencies, and ~5 dB or less at low frequencies, with best agreement in the vicinity of the crossing-point frequency. The strong disagreement for the round jet (SMC000) at high frequencies is an issue for future investigation.

DISCUSSION

Implications to Future Design Efforts

The chevron bend angle effect has been adequately represented by WIND-MGBK in terms of delta-dB influence of chevron inward bend angle. The WIND-MGBK computational method is sufficiently efficient to enable quick turnaround of parametric studies involving chevrons. It follows that the WIND-MGBK approach may be useful in evaluating other jet noise reduction nozzle concepts.

The WIND results show that increasing chevron bend angle leads to thrust loss due to 1) reduced effective nozzle exit area; and 2) reduced flow uniformity (increased divergence) and non-optimum expansion at the nozzle exit. However, the WIND predicted thrust coefficients suggest that the chevron nozzle configurations examined here do not significantly degrade nozzle performance.

SUMMARY

Direct comparisons of WIND-MGBK numerical results with experimental rake, PIV, and microphone data for chevron nozzle configurations have been presented. Despite deficiencies in the RANS model (i.e., underprediction of shear layer maximum TKE levels and related overprediction of core length), the numerical approach is shown to provide reasonably good agreement with the experimentally measured noise trends, for both cold and hot exhaust flow conditions. Most importantly, the delta-dB benefit of chevron inward bend angle is essentially captured. Low–frequency noise levels are reduced while high frequency noise levels increase, for both hot and cold exhaust conditions. The WIND-MGBK methodology may also prove useful in the evaluation of chevron configurations and perhaps other jet noise reduction concepts.

Both the numerical and experimental sensitivity study results indicate that as chevron inward bend angle is increased, mixing is enhanced, resulting in an increase in peak TKE near the jet exit and an earlier breakdown of the core. Thrust penalties for the chevron configurations are numerically predicted to be minimal.

ACKNOWLEDGEMENTS

This work was funded by the Quiet Aircraft Technology (QAT) program at NASA Glenn Research Center under contract C-31035-T. The author thanks Anthony Nerone (NASA GRC) for producing the CAD models and Dr. Nicholas Georgiadis (NASA GRC) for significant technical contributions.

REFERENCES

1. Saiyed, N., Mikkelsen, K.L., and Bridges, J., "Acoustics and Thrust of Separate-Flow Exhaust Nozzles With Mixing Devices for High-Bypass-Ratio Engines," NASA TM 2000-209948, 2000.

2. Saiyed, N., ed., "Separate Flow Nozzle Test Status Meeting," NASA CP-2000-210524, Sept. 1997.

3. Birch, S.F., Lyubimov, D.A., Secundov, A.N., and Yakubovsky, K.Y., "Numerical Modeling Requirements for Coaxial and Chevron Nozzle Flows," AIAA-2003-3287, May 2003.

4. Thomas, R.H., Kinzie, K.W., and Pao, S.P., "Computational Analysis of a Pylon-chevron Core Nozzle Interaction," AIAA-2001-2185, May 2001.

5. Kenzakowski, D.C., Shipman, J., Dash, S.M., Bridges, J.E., and Saiyed, N.H., "Turbulence Model Study of Laboratory Jets with Mixing Enhancements for Noise Reduction," AIAA-2000-0219, Jan. 2000.

6. Koch, L.D., Bridges, J.E., and Khavaran, A., "Mean Flow and Noise Prediction for a Separate Flow Jet with Chevron Mixers," AIAA-2004-0189, Jan 2004.

7. Bridges, J.E. and Brown, C.A., "Parametric testing of chevrons on single flow hot jets," AIAA-2004-2824, May 2004.

8. Nelson, C.C. and Power, G.D., "CHSSI Project CFD-7: The NPARC Alliance Flow Simulation System," AIAA-2001-0594, Jan. 2001.

9. Menter, F.R., "Two-Equation Eddy-Viscosity Turbulence Models for Engineering Applications," *AIAA Journal*, Vol. 32, No. 8, Aug. 1994, pp. 1598-1605.

10. Georgiadis, N., Papamoschou, D., "Computational Investigations of High-Speed Dual-Stream Jets," AIAA-2003-3311, May 2003.

11. Georgiadis, N.J., Rumsey, C.L., Yoder, D.A., and Zaman, K.B.M.Q., "Effects of RANS Turbulence Modeling on Calculation of Lobed Nozzle Flowfields," AIAA-2003-1271, Jan. 2003.

12. Mani, R., Gliebe, P.R., and Balsa, T.F., "High Velocity Jet Noise Source Location and Reduction," *FAA-RD-76-79-II*, 1978.

13. Balsa, T.F., "The Far Field of High Frequency Convected Singularities in Sheared Flows," *J. Fluid Mechanics*, Vol. 74, 1976, pp. 193-208.

14. Wundrow, D.W., Khavaran, A., "On the Applicability of High-Frequency Approximations to Lilley's Equation," NASA/CR-2003-212089, 2003.

15. Khavaran, A., "Role of Anisotropy in Turbulent Mixing Noise," *AIAA Journal*, Vol. 37, No. 7, 1999, pp. 832-841.

16. Kenzakowski, D.C., Papp, J., Dash, S. M., "Evaluation of Advanced turbulence Models and Variable Prandtl/Schmidt Number Methodology for Propulsive Flows," AIAA-2000-0885, Jan. 2000.

Fig. 1: Chevron nozzle on General Electric CF34-8C

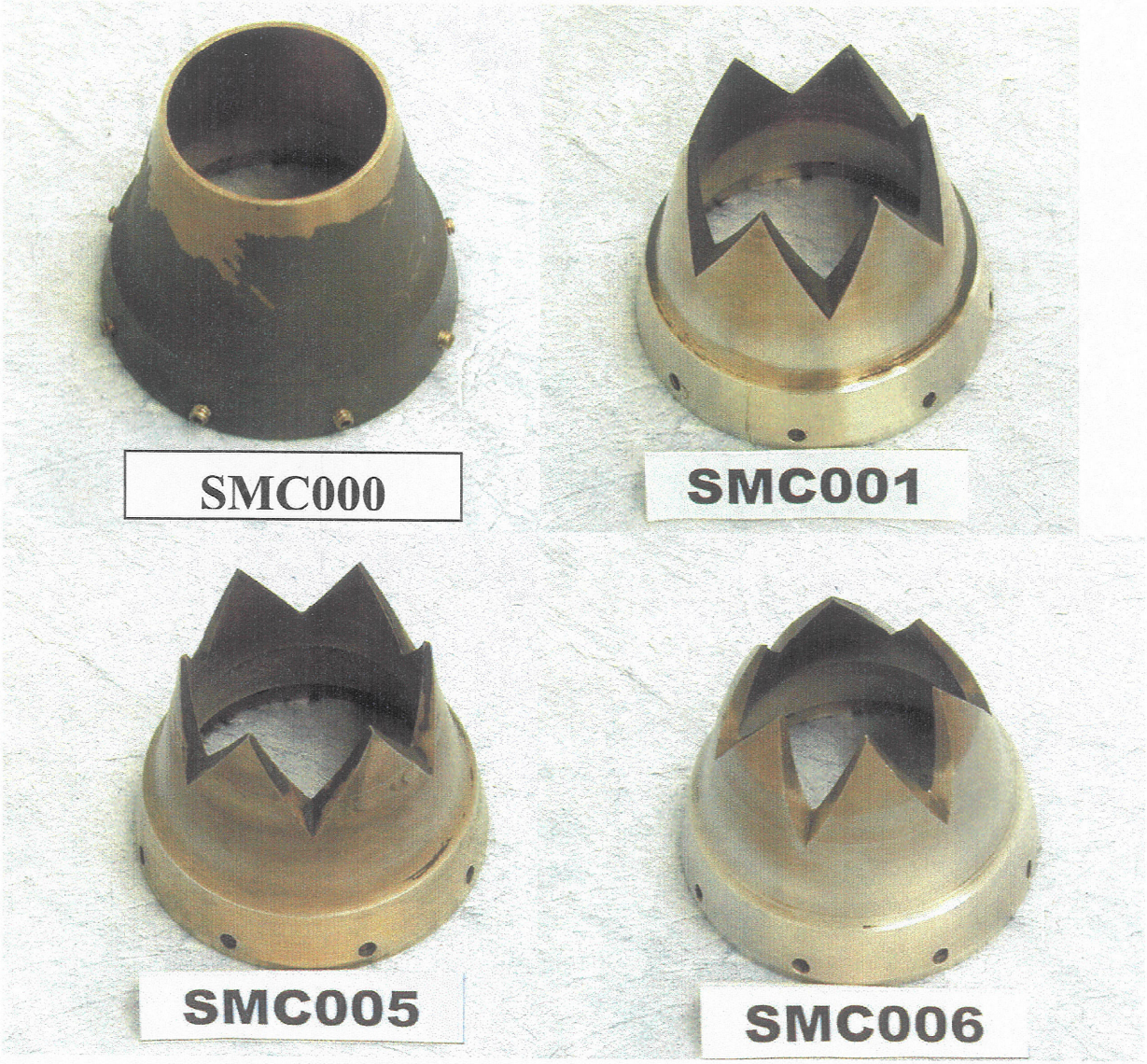

Fig. 2: SHJAR single-stream chevron nozzle configurations

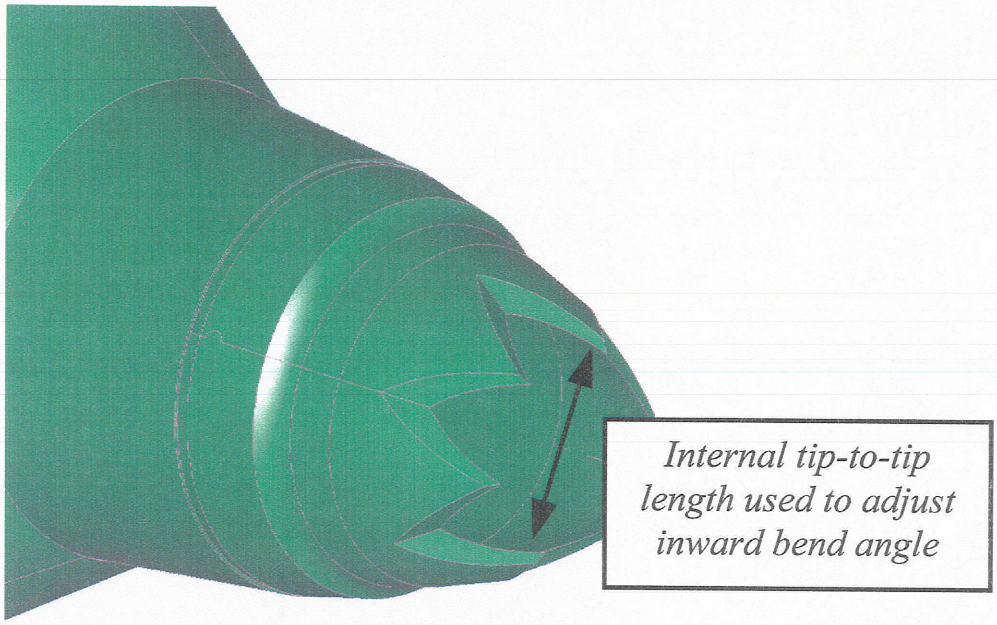

Fig. 3: CAD representation of SHJAR chevron nozzle

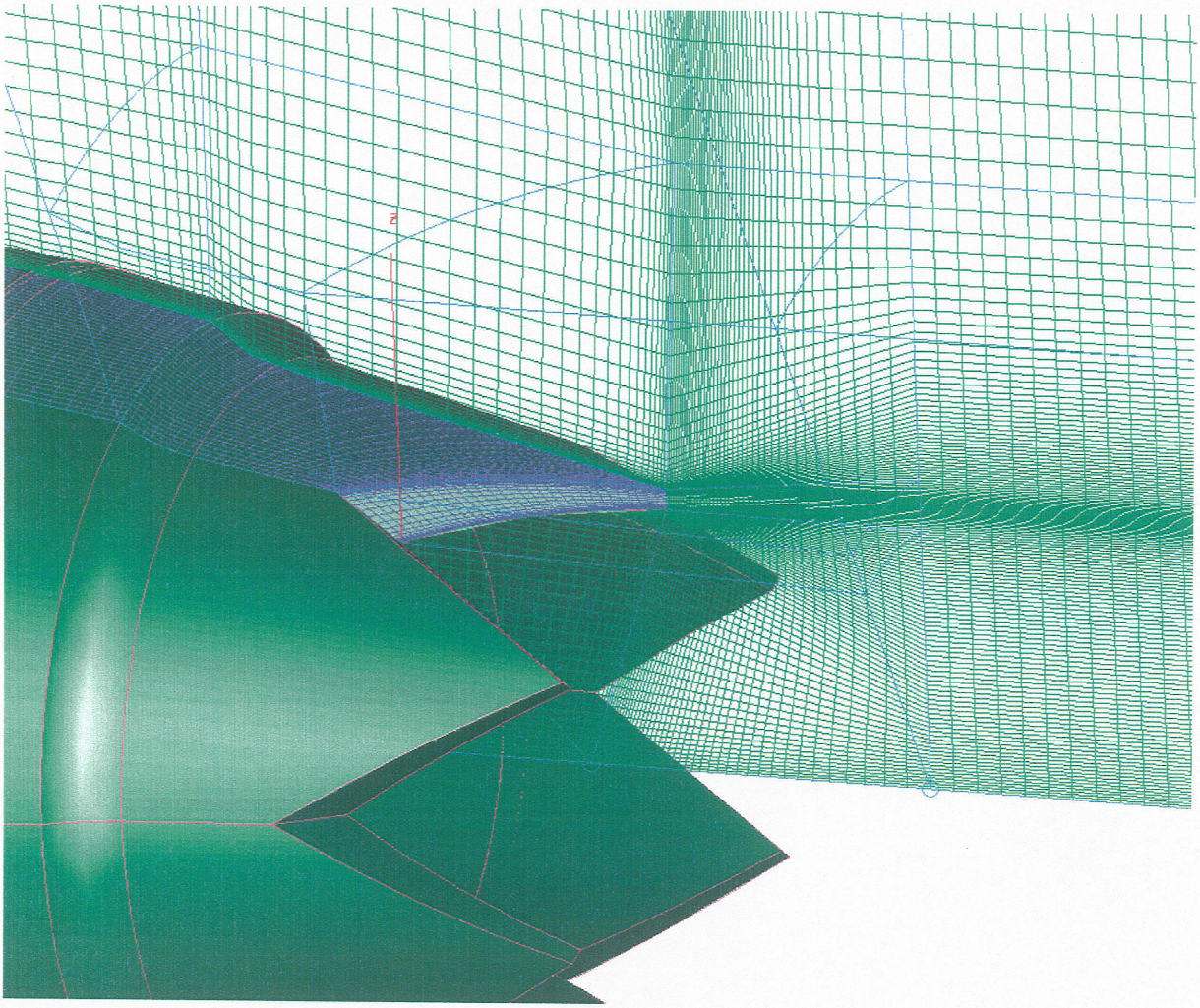

Fig. 4: Sample of SMC001 grid

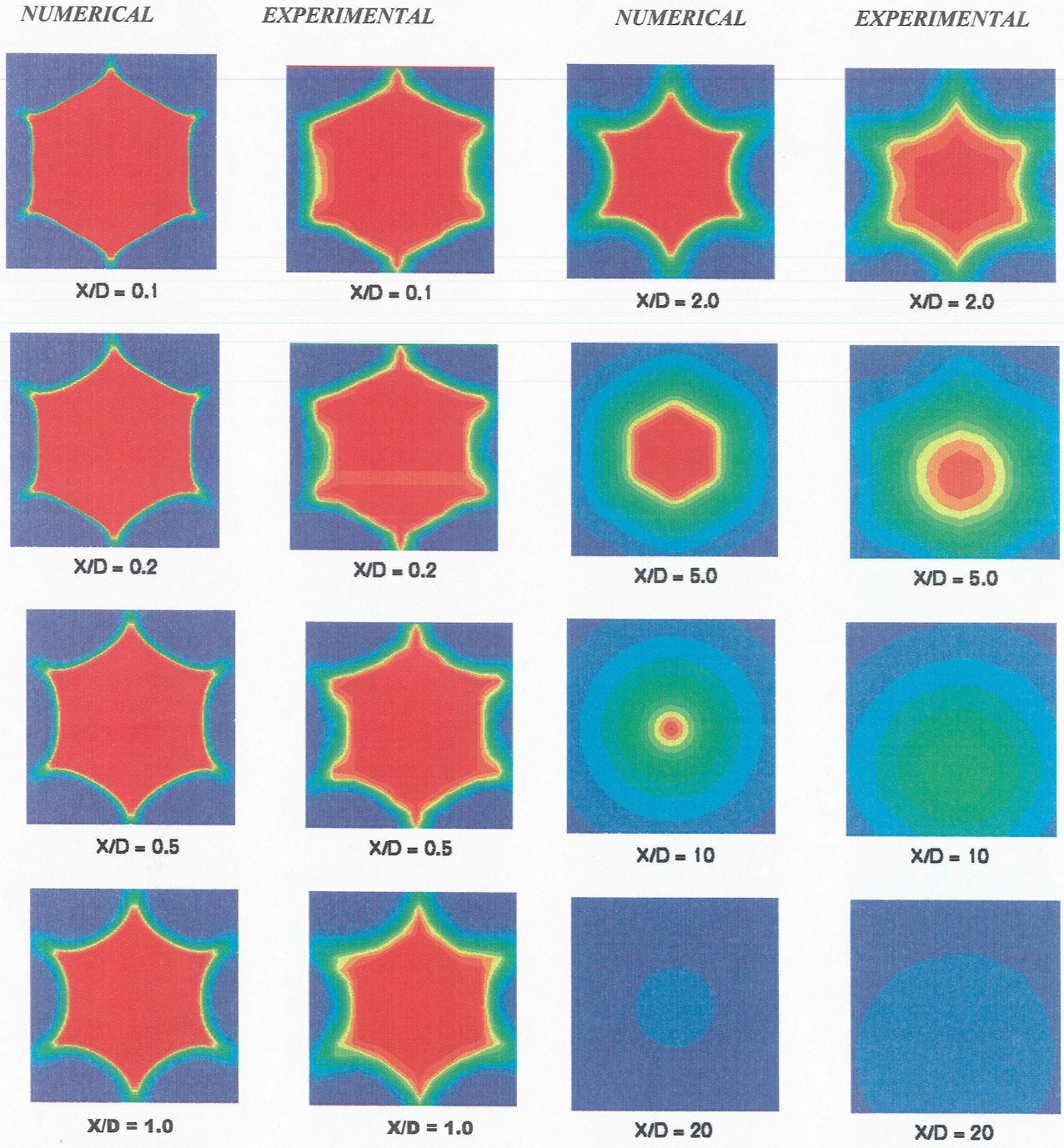

Fig. 5: Stagnation pressure contours at varying axial locations downstream from SMC001 nozzle exit (cold exhaust case)

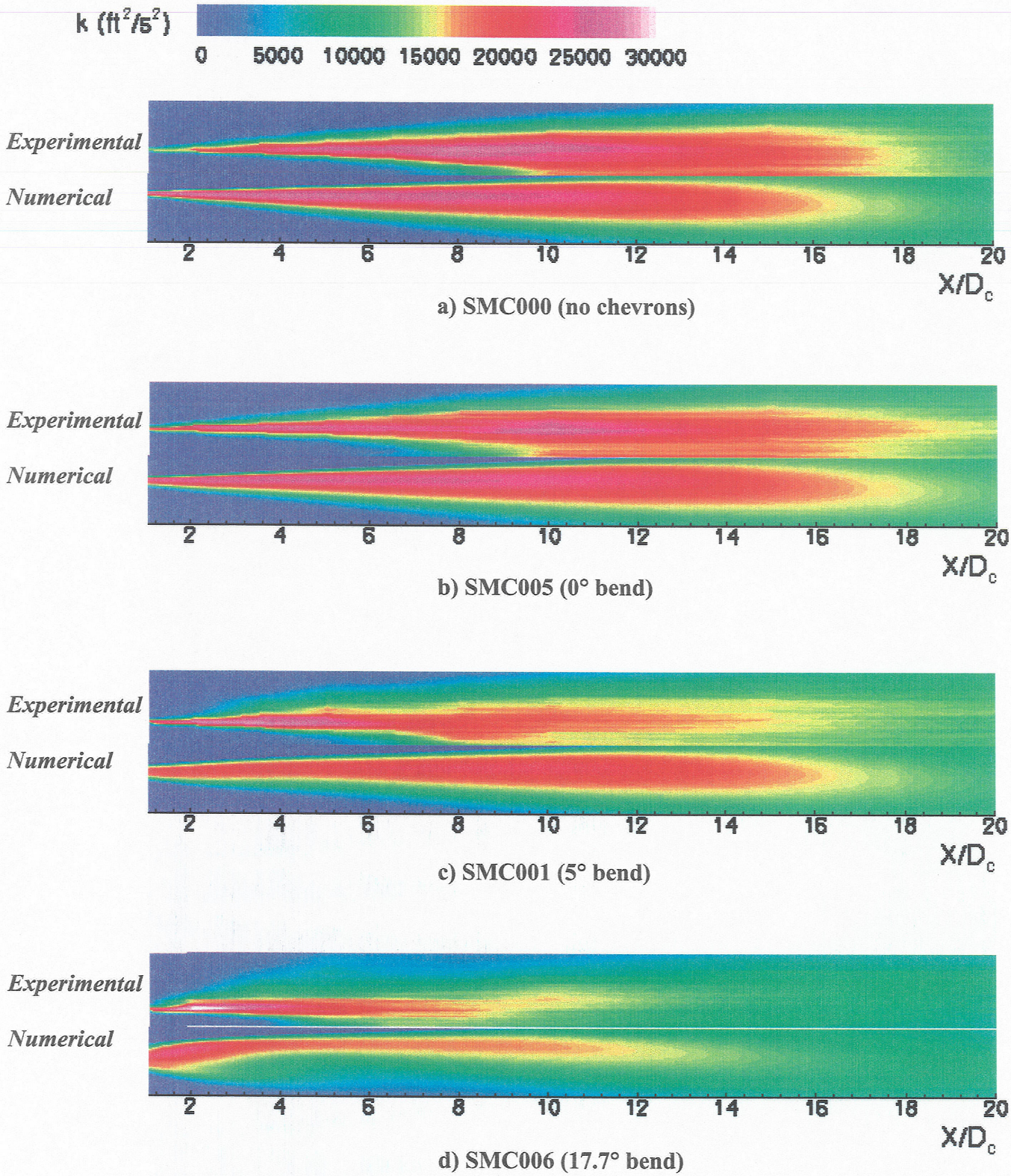

Fig. 6: Comparison of turbulent kinetic energy contours along a planar slice thru chevron center (cold exhaust cases)

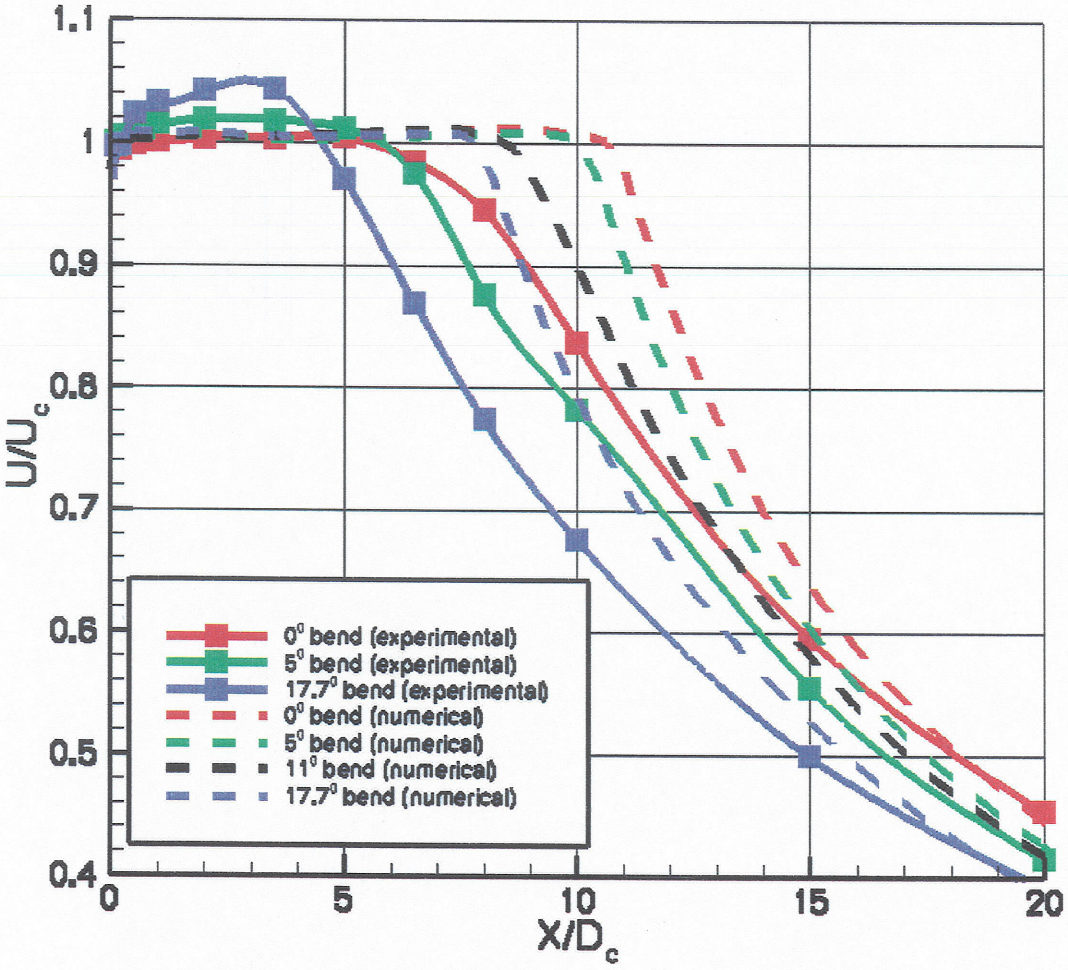

Fig. 7: Centerline velocity contours (cold exhaust cases)

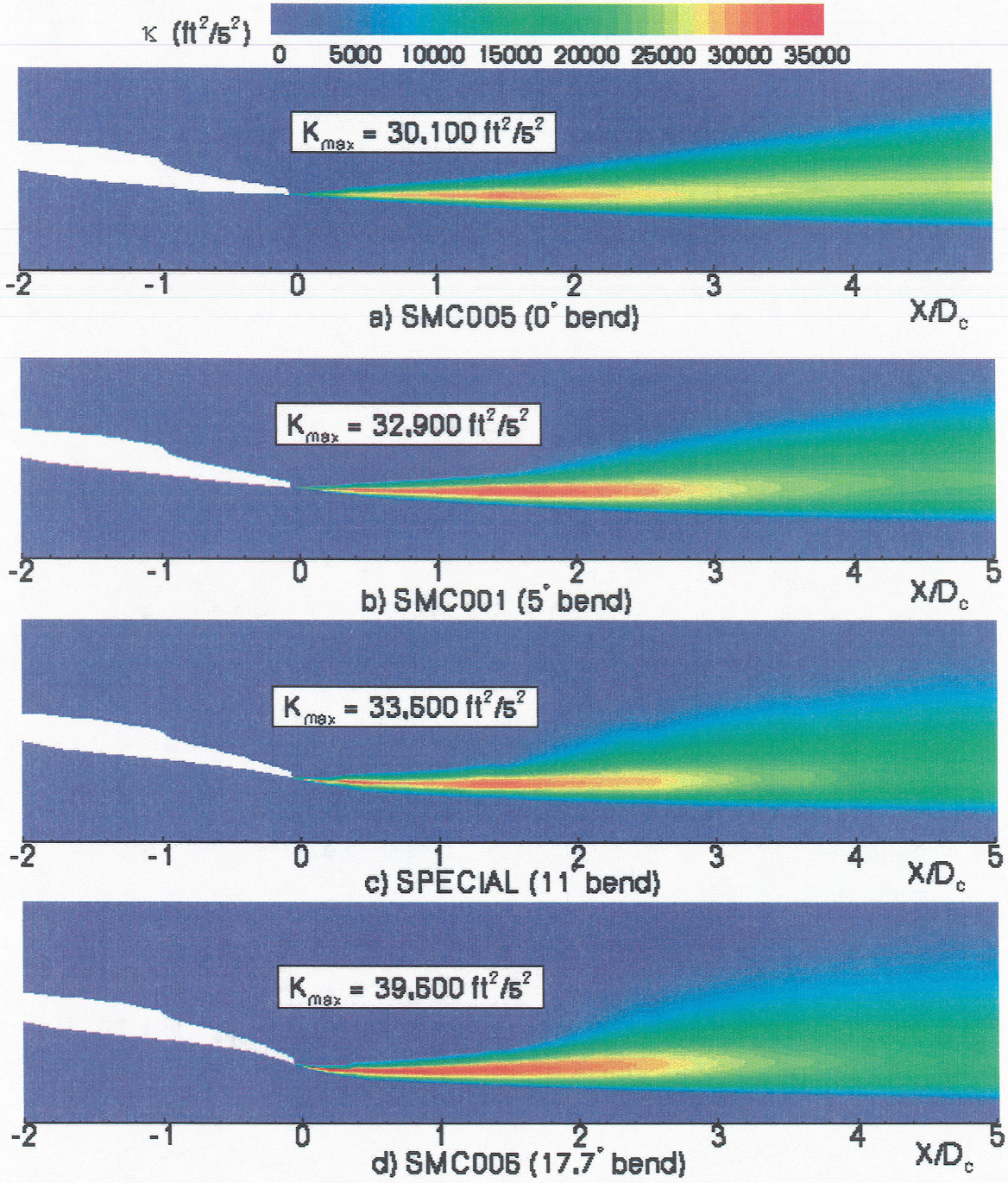

Fig. 8: Turbulent kinetic energy contours along a planar slice thru chevron center (cold exhaust cases)

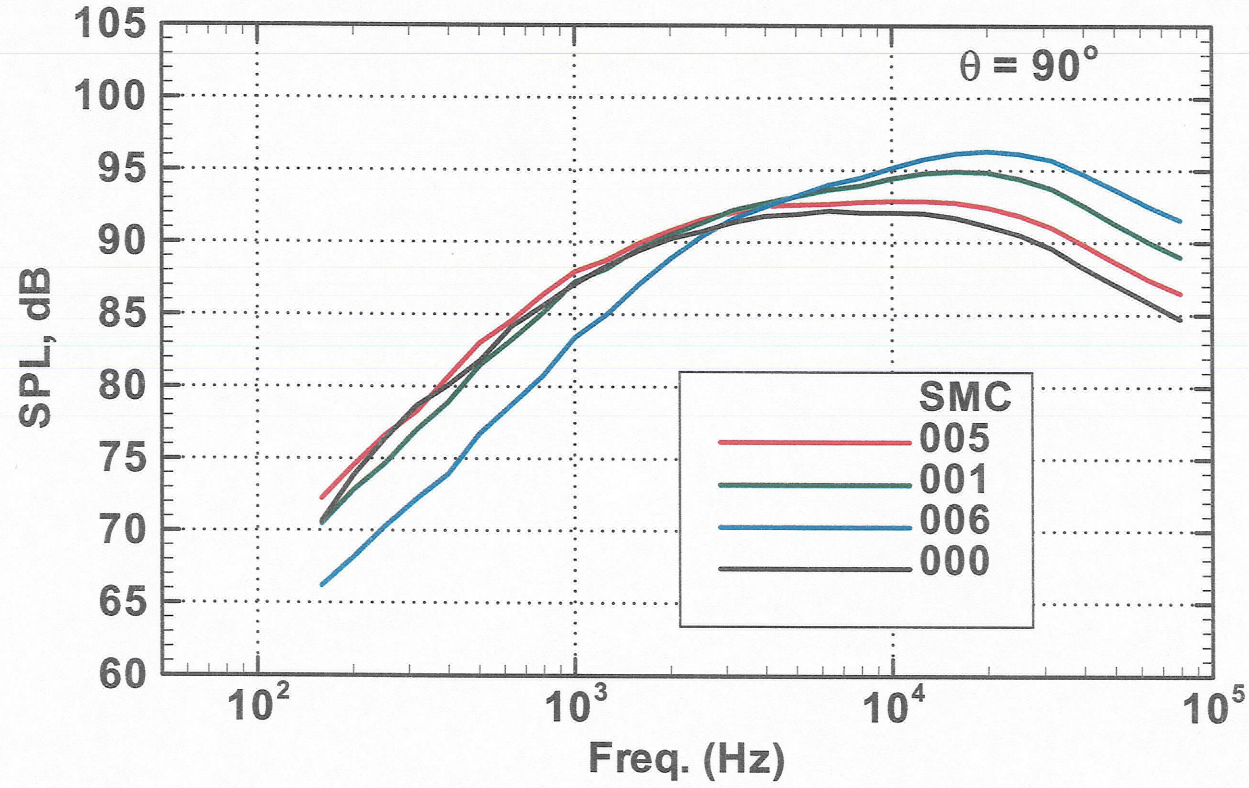

a)

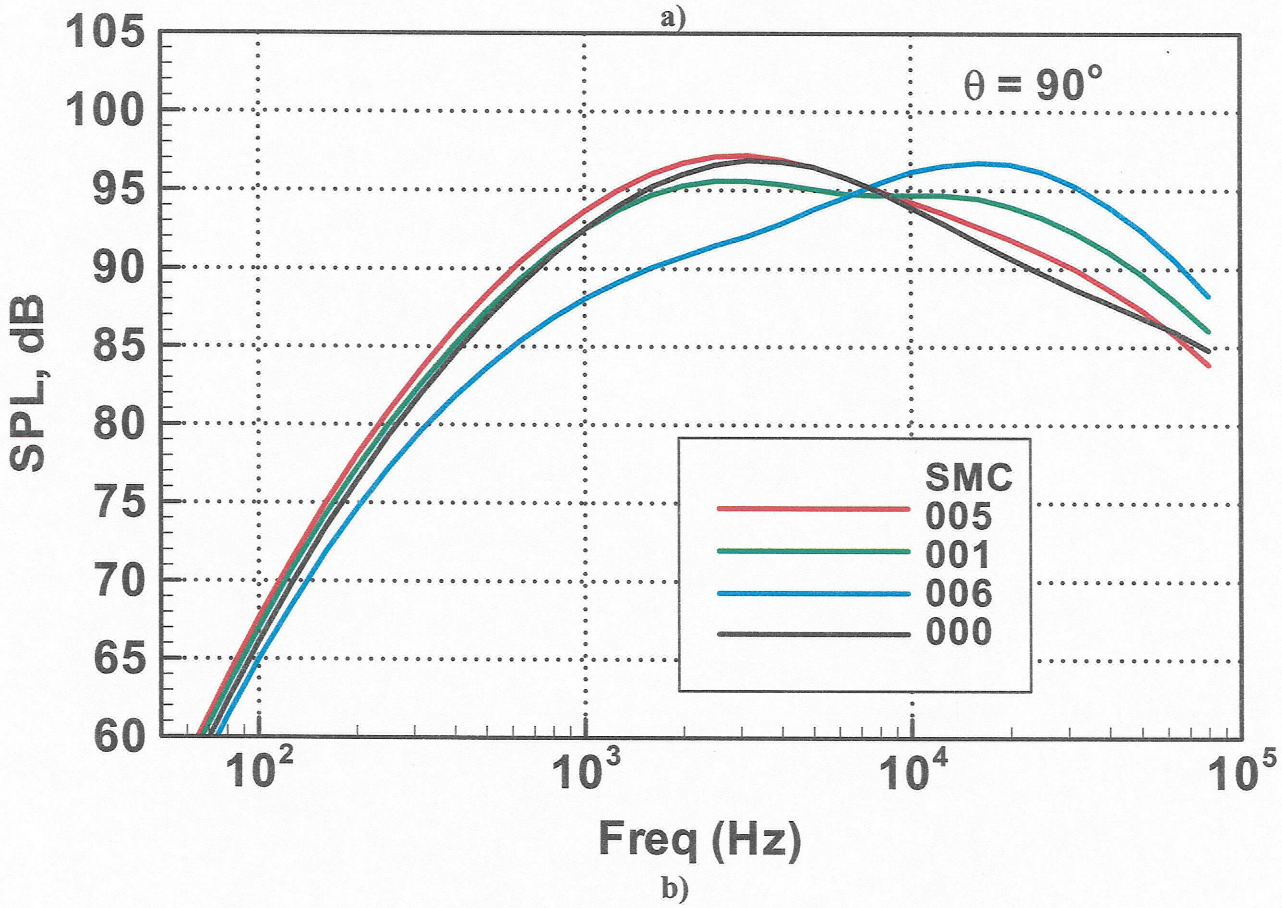

b)

Fig. 9: Numerical vs. experimental noise spectrums at 90° observer angle for cold exhaust cases: a) SHJAR experimental data, b) WIND-MGBK predictions

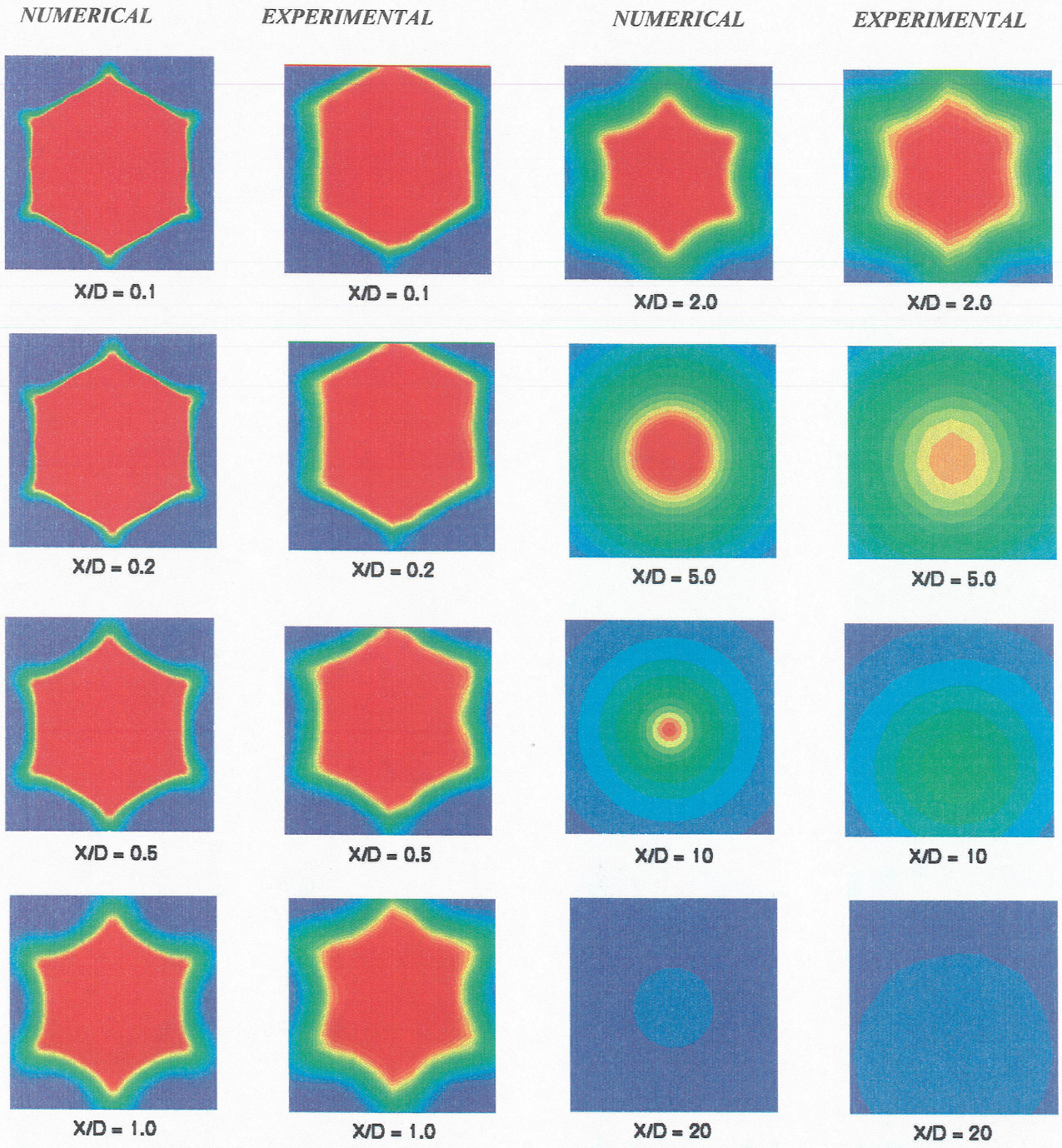

Fig. 10: Stagnation temperature contours at varying axial locations downstream from SMC001 nozzle exit (hot exhaust case)

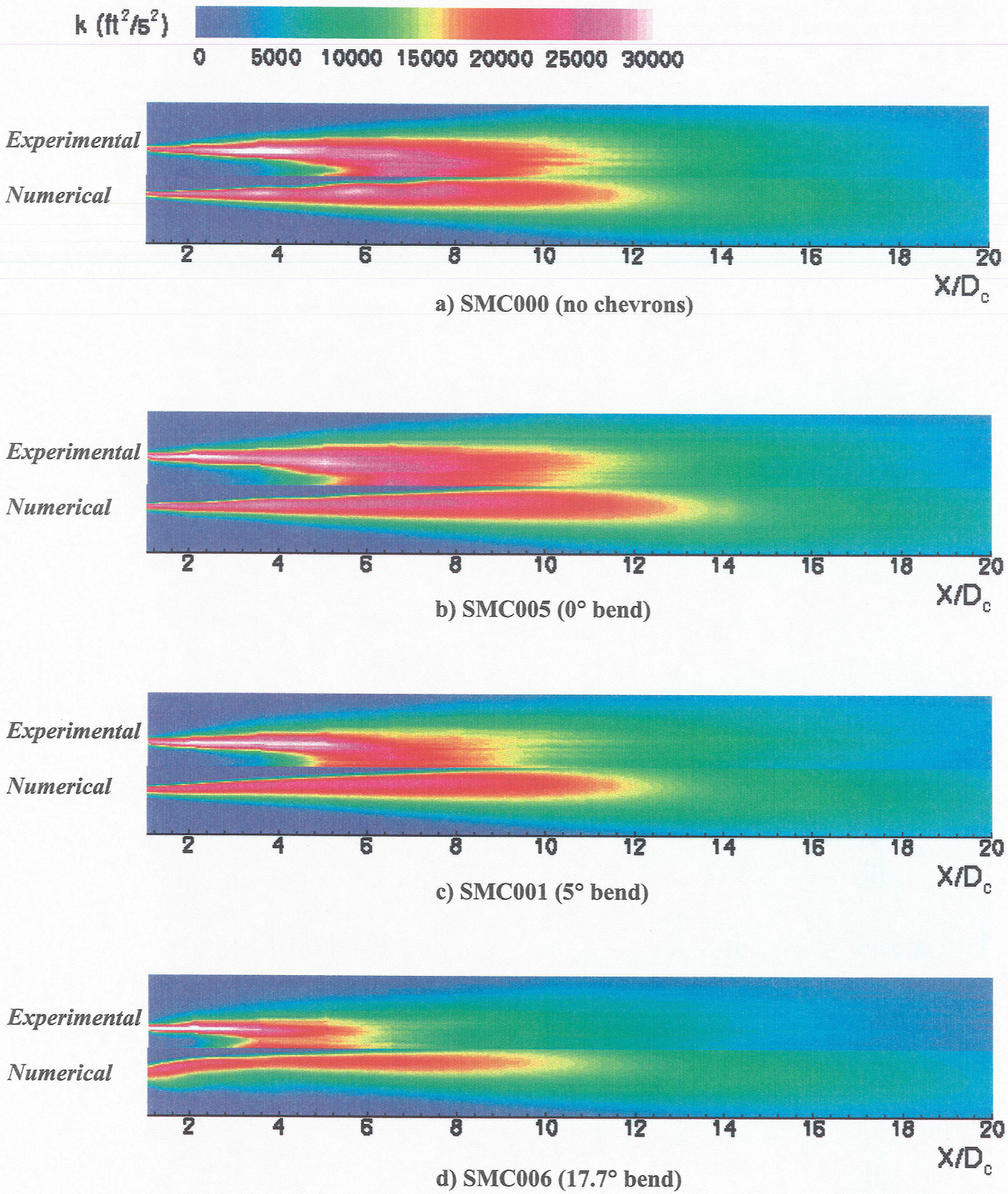

Fig. 11: Comparison of turbulent kinetic energy contours along a planar slice thru chevron center (hot exhaust cases)

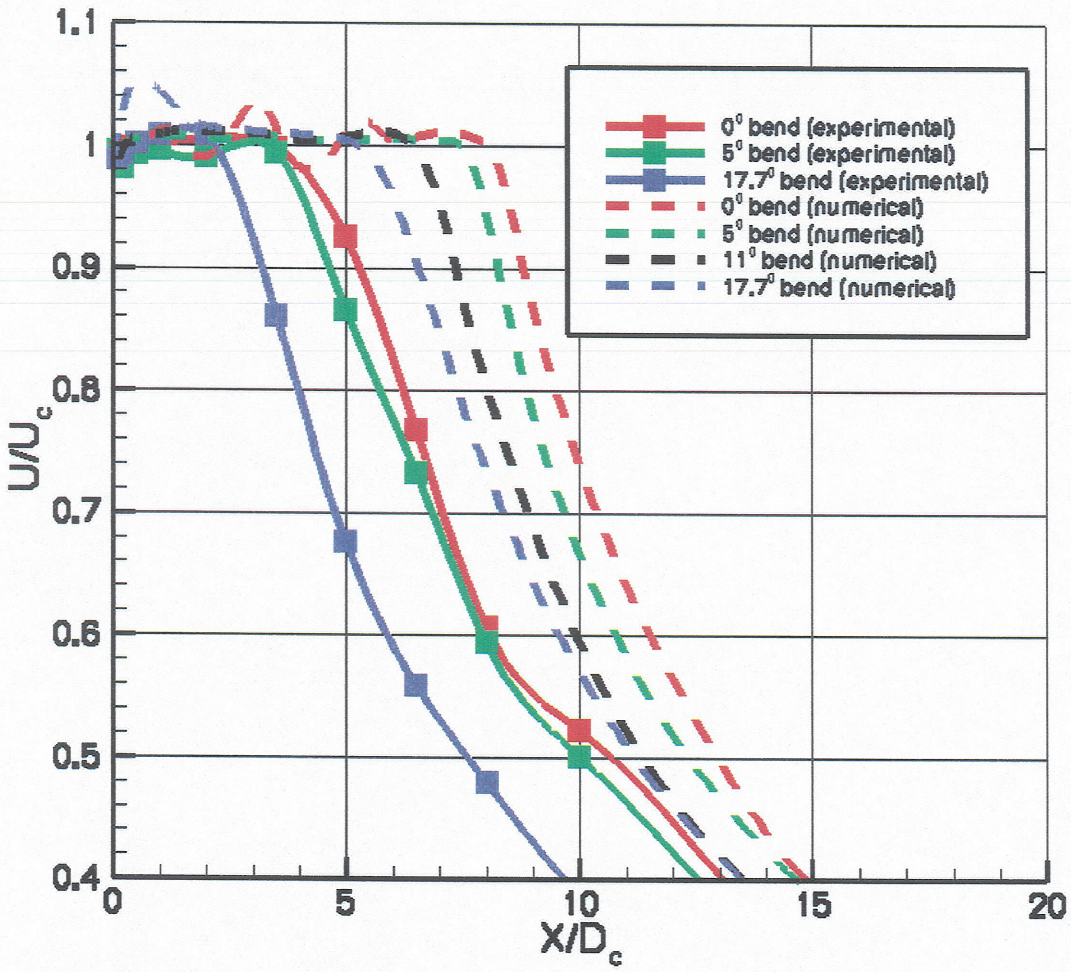

Fig. 12: Centerline velocity contours (hot exhaust case)

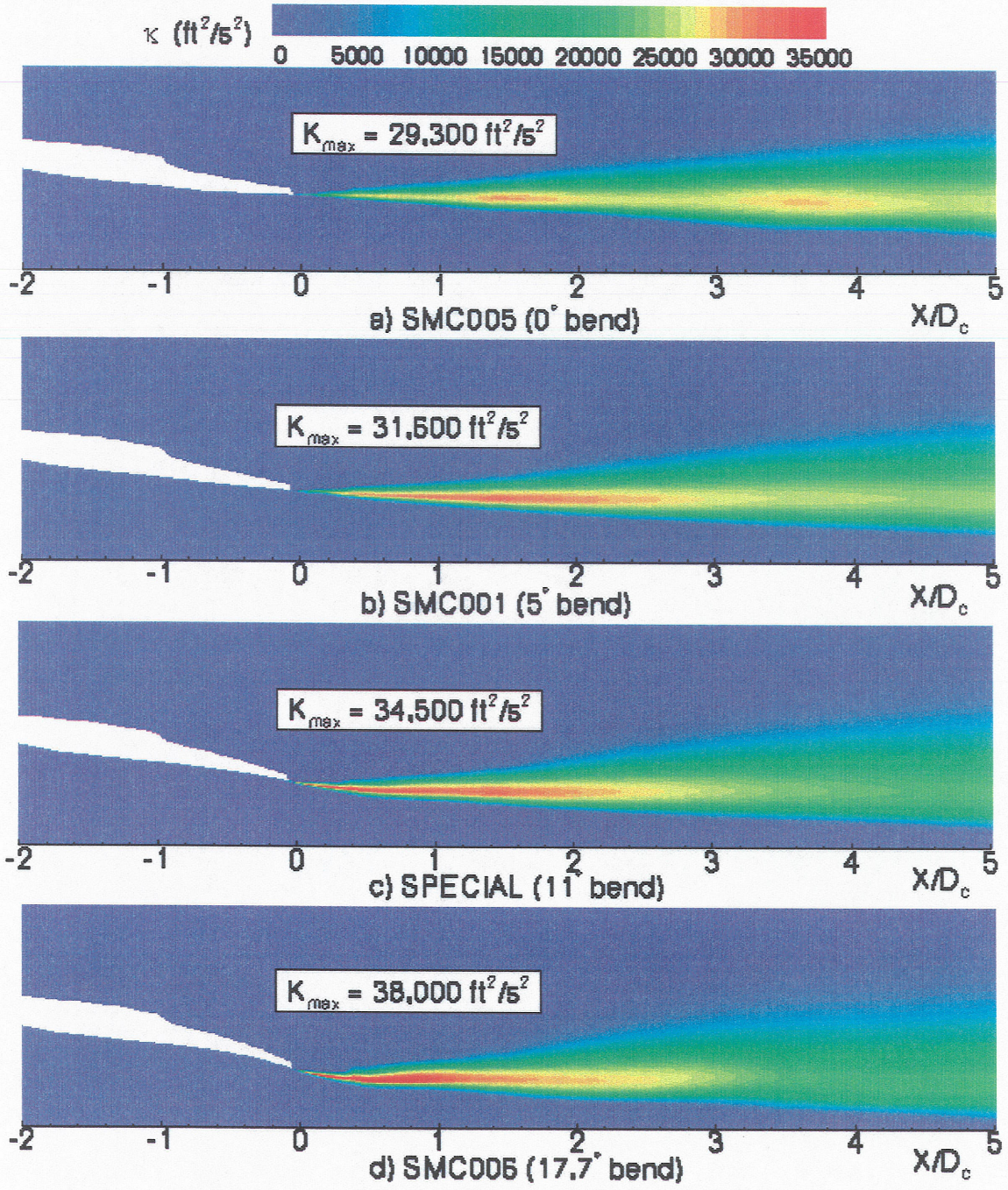

Fig. 13: Turbulent kinetic energy contours along a planar slice thru chevron center (hot exhaust cases)

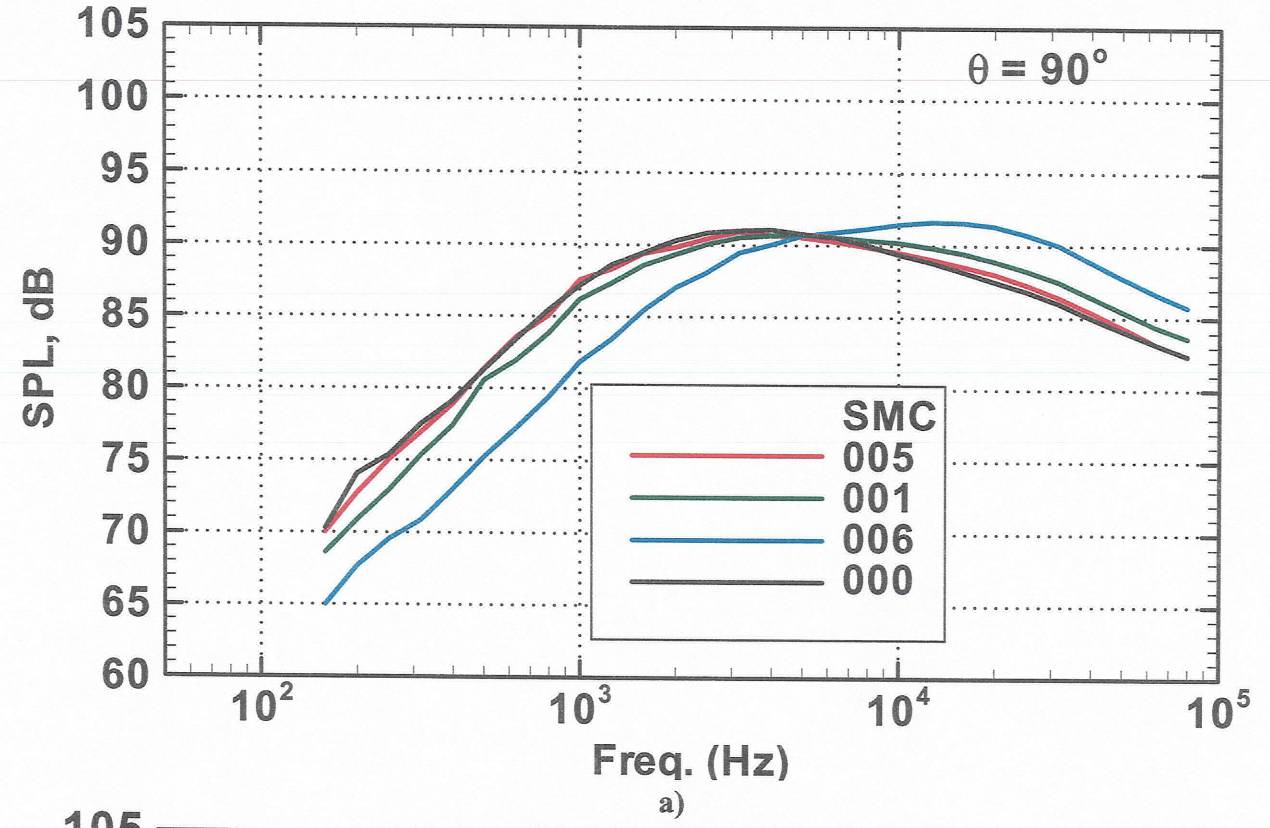

a)

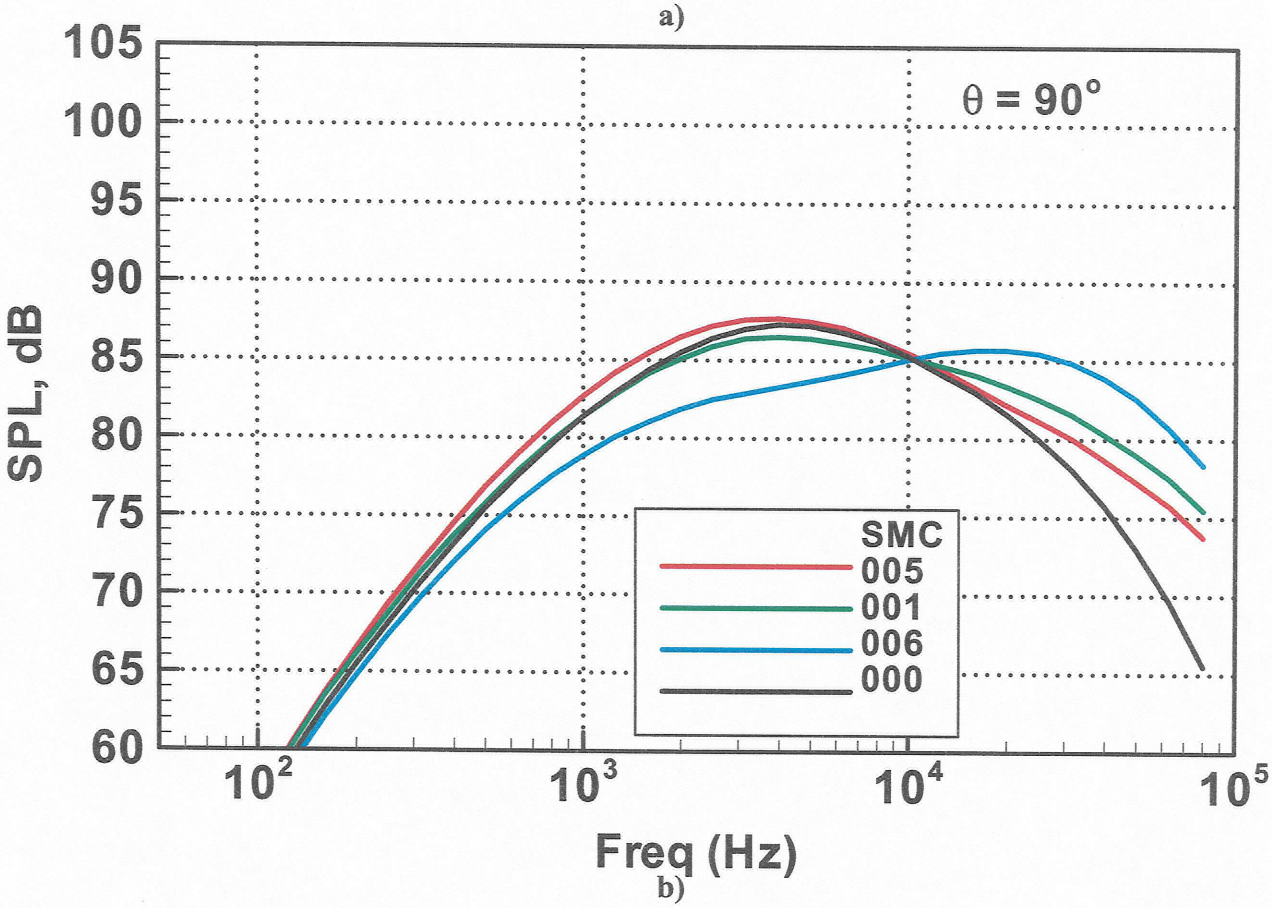

b)

Fig. 14: Numerical vs. experimental noise spectrums at 90° observer angle for hot exhaust cases: a) SHJAR experimental data, b) WIND-MGBK predictions